Zn/Mn co-doped NiO synthesized by sol-gel route for the photocatalytic degradation of methylene blue dye

Sadia Ata,[a] Warda Zaheer,[a] Anila Tabassum,[a] Ijaz Ul Mohsin,[b] Imran Altaf,[c] Aziz ur Rehman,[d] Maryam Al Huwayz,[e] Norah Alwadai,[e] Arif Nazir,*[f] and Munawar Iqbal[g]

This work emphasis on the synthesis of $Ni_{0.2}Mn_{0.02}Zn_{0.02}O$ nanoparticles by facile sol-gel method. The photocatalytic activity was studied for the degradation of methylene blue (MB) dye under the UV light as a function of dye initial concentration, catalyst dose and pH of the medium. Scanning electron microscopy (SEM) and energy dispersive X-ray (EDX) were utilized for the study of morphological and elemental composition, while XRD analysis was employed for structural study of the prepared material, which formation the phase purity and size was in 20–24 nm range. The bandgap of Zn/Mn co-doped NiO NPs (3.24 eV) was reduced as compared to pure NiO NPs (3.43 eV). The degradation efficiency of pure NiO NPs and Zn/Mn co-doped NiO NPs was found to be 70% (60 min) and 94% at optimum conditions. The dielectric properties were also studied, which were also improved in response of doping. The findings revealed that the optical and catalytic properties of Zn/Mn co-doped NiO NPs were improved versus pure NiO NPs, which could be employed for the remediation of dyes in effluents.

Introduction

Environmental pollution refers to the introduction of harmful substances and pollutants into the natural environment, leading to adverse effects on living organisms and ecosystems. This pollution can occur in various forms, affecting the air, water, soil, and even the overall climate.[1,2] Only 3% of the Earth's water is suitable for essential purposes such as drinking, household use, and industrial activities. This limited freshwater resource is as crucial to life as oxygen is for living organisms. Water is considered healthy or "Blue Gold" when it is free from harmful pathogens, dangerous chemicals, and industrial pollutants. Unfortunately, various industries, including textile, leather dyeing, and food processing units, significantly contribute to water contamination. Population growth, urbanization, and rapid industrialization also play a major role in polluting our water bodies. The scarcity of clean water and its significance to life make it imperative to protect and preserve this precious resource from contamination caused by human activities and industrial processes.[3,4] Annually, synthetic dyes are being produced in a huge quantity and 15% of them are discharged into water. The dyes are the persistent molecules, which affect the environment and living organisms adversely.[5,6]

These dyes affect the living organisms depending upon their duration of exposure time by causing malignant neoplastic diseases and high incidents of bladder cancer. Adding more, they effect the nervous system and can cause inactivation of the enzymes such as enzyme cofactor inhibition. Shortness of breath, headache, confusion and high arterial pressure in humans is caused by cationic methylene dye (MB) along with serotonin syndrome, lysis of erythrocytes and many allergies. In humans, it also causes blindness, shock, tissue necrosis.[7,8] Its prolonged contact can cause itching and redness of skin. In aqueous conditions, even at low concentration, it can produce colored products having high molar absorption, causing reduction in light transmittance, decreasing oxygen solubility and eventually effecting the photosynthesis.[9]

Hence, it is essential to eliminate dyes because of their many adverse effects on living organisms. Many techniques like adsorption method, coagulation/flocculation, and precipitation are used, which need long operational time and secondary products are also produced from dyes.[10] Therefore, some

[a] *Dr. S. Ata, Dr. W. Zaheer, Dr. A. Tabassum*
School of Chemistry
University of The Punjab
Lahore, Pakistan

[b] *Dr. I. Ul Mohsin*
Institute of Applied Materials-Applied Materials Physics (IAM-AWP)
Karlsruhe Institute of Technology
Karlsruhe, Germany

[c] *Dr. I. Altaf*
Institute of Microbiology
University of Veterinary and Animal Sciences
Lahore, Pakistan

[d] *Dr. A. ur Rehman*
Department of Chemistry
Islamia University of Bahawalpur
Bahawalpur, Pakistan

[e] *Dr. M. Al Huwayz, Dr. N. Alwadai*
Department of Physics
College of Sciences
Princess Nourah bint Abdulrahman University
P.O. Box 84428, Riyadh 11671, Saudi Arabia

[f] *Prof. Dr. A. Nazir*
Department of Chemistry
The University of Lahore
Lahore, Pakistan
E-mail: anmalik77@gmail.com

[g] *Dr. M. Iqbal*
Department of Chemistry
Division of Science and Technology
University of Education
Lahore, Pakistan

advanced and destructive methods are required for the removal of dyes form wastewater. The photo-catalysis has been emerged as an evident choice for the practical field applications among the AOPs with no secondary pollutants and without any dangerous side products. For the removal of complex dyes, this technique proved to be environment friendly and highly efficient without generating the secondary pollution issues.[11,12]

Nanoparticles have size ranging from 1–100 nm manifested improved physico-chemical properties due their large surface area and imported optical properties.[13] The metal oxide nanoparticles, doped and composite materials reported to be highly efficient for the photocatalytic removal of dyes.[14] NiO nanoparticles are one of the important p-type semiconductors with band gap ranging from (3.5–4.0) eV. These nanoparticles have various applications as gas sensors, in the construction of smart windows, electrochromic displaying instruments, in lithium batteries, magnetic materials and photovoltaic devices, in ceramic materials and solar cells. NiO NPs as a photocatalyst degrade the contaminants by oxidation processes, using high oxidative potential (2.7 and −2.3 eV) reactive oxygen oxides and hydroxides radicals.[15] For the synthesis of NiO nanoparticles different methods like hydrothermal, co precipitation, micro-emulsion, sol-gel, sputtering and laser ablation were used. In this work, nanoparticles were prepared using sol-gel method and the properties of the material was controlled by monitoring the conditions (such as reaction time, temperature or precursor salts) and hence different size of materials can be created. Low temperature is required with more yield at the end. We can introduce small amount of dopants and in final product uniformly. To get maximum performance from a catalyst (NiO) at its optimum conditions, a detailed investigation has been reported as a photo nanomaterial for the dye degradation. Cu doped NiO particles,[16] facile synthesis of NiO-ZnO–Ag nanocomposites and biosynthesized NiO particles showed improved efficiency in dye eradication from water. Synthesis of Fe doped and other transition metals doped nickel oxide particles has also been reported.[17] In order to improve the structure, optical and magnetic properties, Mg doped NiO nanoparticles were reported with reduced band gap and improved crystallinity.[18] By doping Zn in NiO crystals its bandgap decreased with promising efficiency in the visible region. Improved properties of NiO crystals were also reported after doping of Mn transition metal.[19]

Zn metal doping showed reduction in bandgap, more activity in visible region and increased capacitance.[20] Doping with Mn exhibited more stability, more charge separation and extend in light absorption ranges. The choice of precursor compounds can be influenced by various factors, including the desired properties of the final material, the synthesis method, and the stability and reactivity of the precursors. Chloride-based precursors, such as nickel chloride and manganese chloride, are often chosen for certain applications because they can readily decompose at relatively low temperatures to yield the corresponding metal oxides or other compounds. These precursors may be preferred for certain synthesis techniques, like sol-gel methods or precipitation reactions, where low-temperature processing is desired. On the other hand, metal nitrates, like zinc nitrate, are commonly used as precursors because they are generally more stable than their chloride counterparts and can be easily dissolved in various solvents. This makes them suitable for processes like chemical solution deposition or spray pyrolysis. Doping NiO with Zn and Mn is a common practice to modify the properties of the material and enhance its performance for various applications. By incorporating Zn and Mn atoms into the NiO lattice, the electronic structure and physical characteristics of the material can be altered, leading to improvements in its electrical, magnetic, and optical properties.[21]

Based on aforementioned facts, the objective of this study was to synthesize pure and Zn/Mn co-doped nanoparticles by facile sol-gel method and their application as a photocatalyst for MB dye degradation along with optimization for process variable as well as dielectric properties evaluation of the Zn/Mn co-doped NiO versus pure NiO nanoparticles.

Results and discussion

UV-Vis analysis

The electronic excitation spectra of NiO and Zn/Mn co-doped NiO NPs was recorded in the range of 200–600 nm (Figure 1a, b). The maximum absorbance of pure NiO NPs was recorded at 287 nm, while the doped NiO nanoparticles showed peak at 323 nm, clearly demonstrated a red shift in the absorbance value.[22] Davis and Moff expression was used to calculate optical bandgap (Eq. 1).

$$ahv = a_0(h_v - Eg)^n \quad (1)$$

Where, α is absorption coefficient, α_o is energy dependent constant, h is Planck's constant, $n = {}^1/_2$ is power factor for transition mode ($^1/_2$ and 2 for allowed direct and indirect transitions, 3/2 and 3 for forbidden direct and indirect transition). The extrapolation of linear region of the plot between $(\alpha h\upsilon)^2$ versus photon energy gave the value of bandgap that was 3.43 eV for NiO and 3.24 eV for the Zn/Mn co doped NiO NPs (Figure 1c, d). The bandgap energy value has been decreased for Zn/Mn co doped NiO nanoparticles, indicated a smaller space or lattice contraction induced by the generation of vacancies and energy states upon doping (Zn and Mn) metals.[23] Similar effect was also studied by Barman et al[24] and Dewan *et al.*[25] for doping Mn and Zn on NiO nanoparticles, respectively. Also, doping of other metals like Co, Fe doped NiO particles by wet method reported the decrease in bandgap values.[26] This reduced bandgap was an actual cause of high efficiency of the prepared samples and hence, proved them an active photocatalysts for dye degradation. The doped metals (Zn and Mn) are likely to play a crucial role in the photocatalytic process as entrapped sites. The introduction of dopant metals into the parent material can create localized energy states within the bandgap. These energy states arise due to the differences in the ionic radii of the dopant metals (Mn, and Zn) compared to the host material. The dopant metals

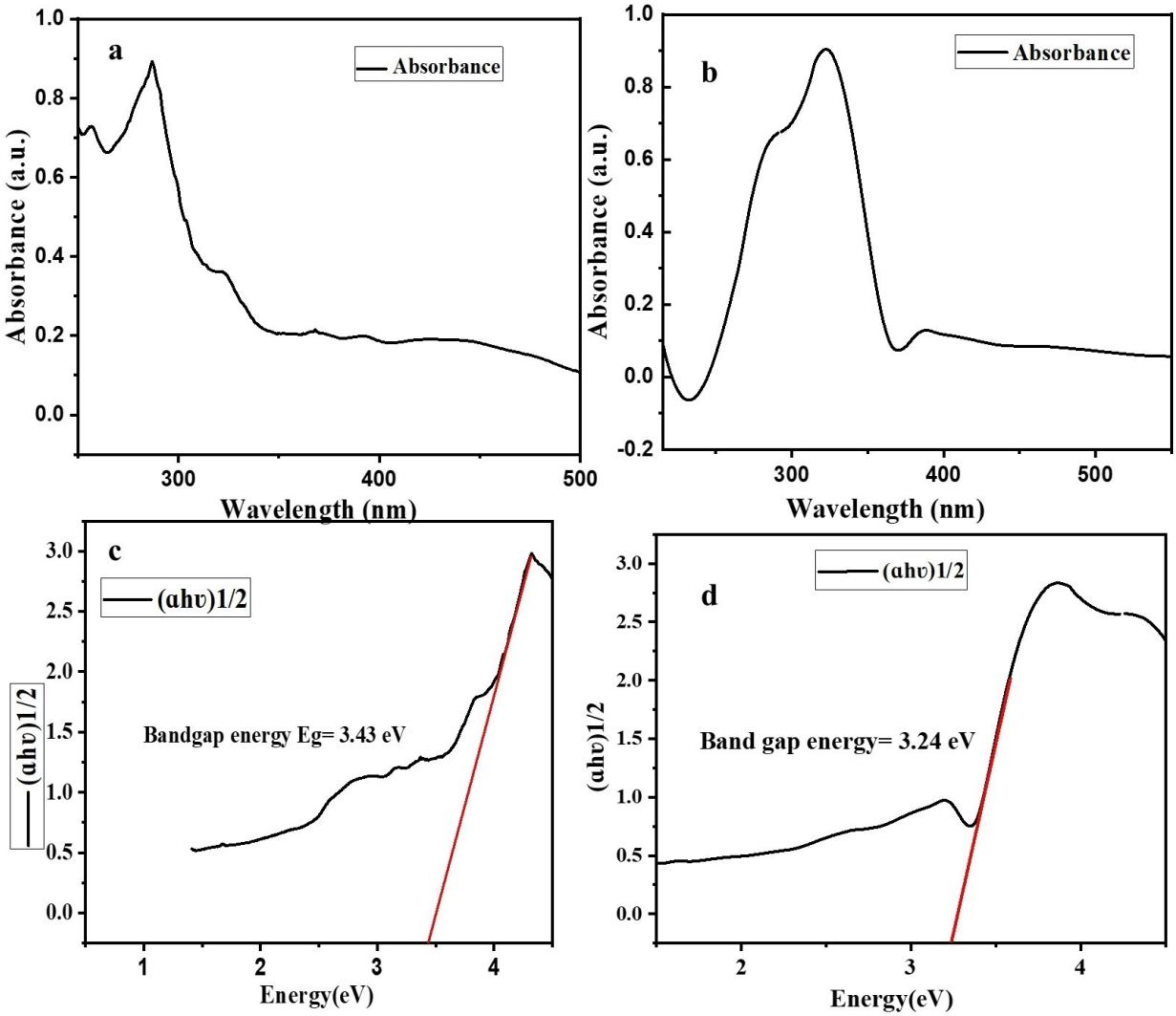

Figure 1. UV-Vis spectra of (a) pure NiO NPs, (b) co-doped material, (c) Energy bandgap of NiO NPs and (d) Energy bandgap of co-doped nanoparticles.

can cause changes in the electronic structure of the parent material, leading to modifications in its bandgap. The bandgap reduction is a significant factor that enhances the photocatalytic activity of the material. By narrowing the bandgap, the doped material becomes more sensitive to light, allowing it to absorb a broader range of wavelengths, including visible light, which is abundant in solar radiation. This increased light absorption promotes the generation of electron-hole pairs, which are crucial for photocatalytic reactions. Moreover, the presence of dopant metals introduces trapping or interstitial energy levels within the parent material.[27] These additional energy levels provide sites for the migration and trapping of charge carriers (electrons and holes) generated during the photocatalytic process. As a result, the dopants act as centers for charge separation and facilitate the efficient utilization of photoinduced electrons and holes in redox reactions with target pollutants, thus improving the overall photocatalytic performance. Considering the ionic radius differences between the dopant metals (Ni, Mn, and Zn), the specific dopant chosen (Zn or Mn) can lead to different effects on the band structure and trapping behavior of the parent material.[28] The choice of dopant impacts the photocatalytic performance and consider the optimal doping concentration to achieve the desired bandgap reduction and efficient charge carrier utilization. Hence, the incorporation of Zn and Mn as dopants in the parent material is likely to enhance the photocatalytic process by creating entrapped sites for charge carriers and reducing the bandgap. The selection of suitable dopant metals and their concentration is crucial to achieving an efficient and effective photocatalytic material for environmental remediation and other applications.

Surface morphology

Surface morphology of the pure NiO (Figure 2a–c) and Zn/Mn co doped (Figure 2d–f) NiO was revealed by SEM images. The pure and Zn/Mn co deoped NiO exhibitted wafers shape surface morphology with agglomeration. The agglomeration mainly arises owing to the insignificant particle size linked to high

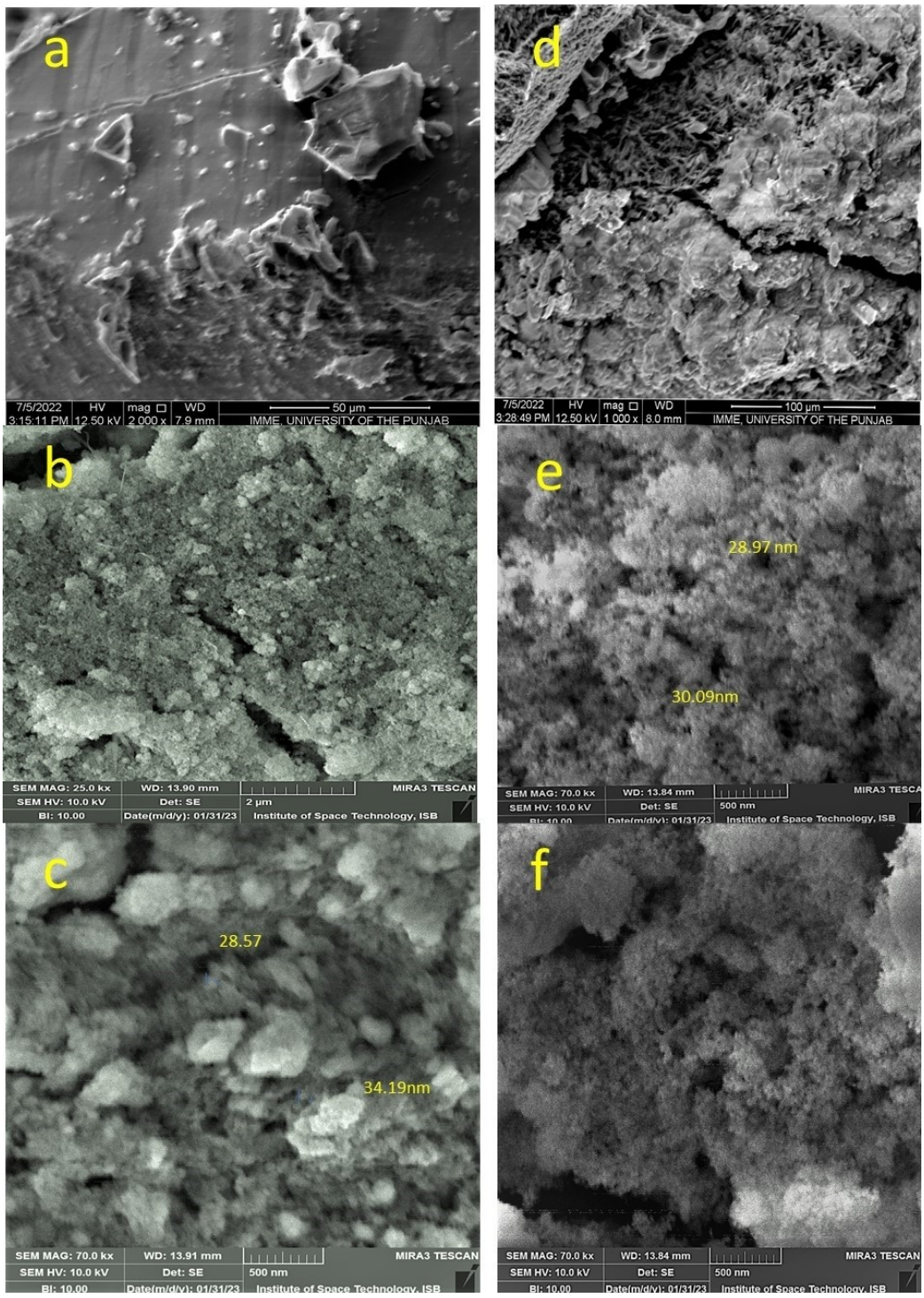

Figure 2. Scanning Electron Microscopy images of pure (a,b,c) and co-doped (d,e,f) NiO NPs.

superficial energy. In addition, doping of Zn an Mn metal ions cause lattice distrotions which leads to the morphological changes. The average size of the NiO and Zn/Mn co-doped NiO determind from the SEM analysis is around 31 and 28 nm, respectively.[29] Furthermore, the elemental analysis of the was done by EDX (Figure 3a, b). The EDX spectra approves the presence of Ni and O in pure NiO NPs. On the other hand, Mn and Zn metals are also detected in the co-doped material. The results suggested the uniform dispersion of Zn and Mn metal ions in the NiO matrix. Atomic and weight percentage of the elements confirmed the the presence of respective elements in nanoparticles.

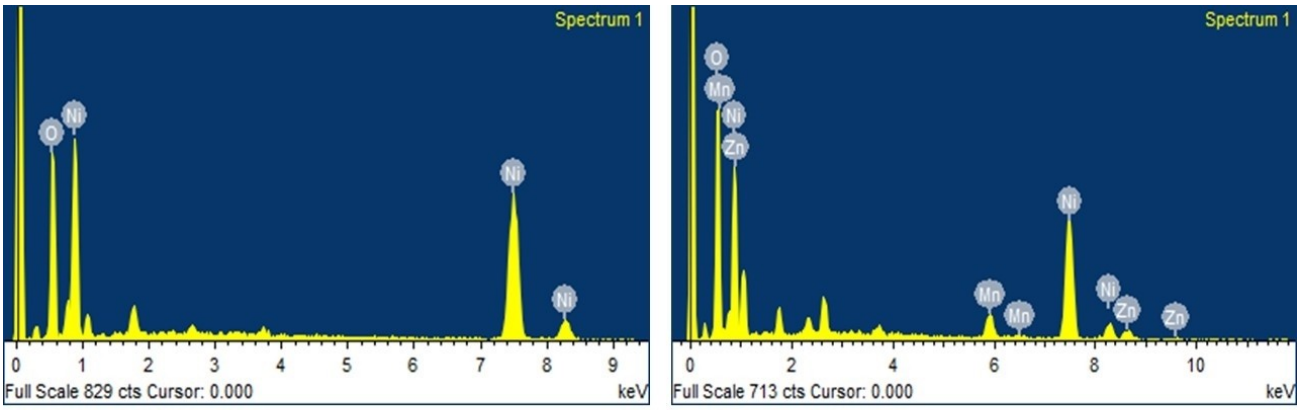

Samples	Ni (at. %) \ wt. %	O (at. %) \ wt. %	Zn (at. %) wt. %	Mn (ar.%) wt. %
Pure NiO	69.38 \ 38.18	30.62 \ 61.82	–	–
Doped NiO	53.44 \ 27.56	35.28 \ 66.76	6.15 \ 2.85	5.13 \2.83

c

Figure 3. (a) EDX of NiO NPs and (b) co-doped NPs (c) composition of the synthesized nanoparticles.

FTIR analysis

FTIR analysis was used for the evaluation of functionalities in the prepared samples (Figure 4). It showed characteristics bands at specific wavenumbers that indicated the presence of functional groups. FTIR spectrum of the NiO NPs and Zn/Mn co-doped NiO NPs was observed in the wavenumbers range of 400–4000 cm^{-1}. The peaks found at 3372 and 1652 (cm^{-1}) represented the O–H stretching and bending vibrations respectively (Table 1).[30] The wideness of peak at 3372 cm^{-1} (3300–4000 cm^{-1}) was because of the water molecules adsorbed on the surface of the materials. Peak at 2938 cm^{-1} expressed the existence of hydroxyl ions. Peaks at 1446 and 1051 (cm^{-1}) corresponded to the existence of oxides group. The peaks present in the range of 530–860 cm^{-1} were due to the lattice enlargement and defects in the crystal which occurred

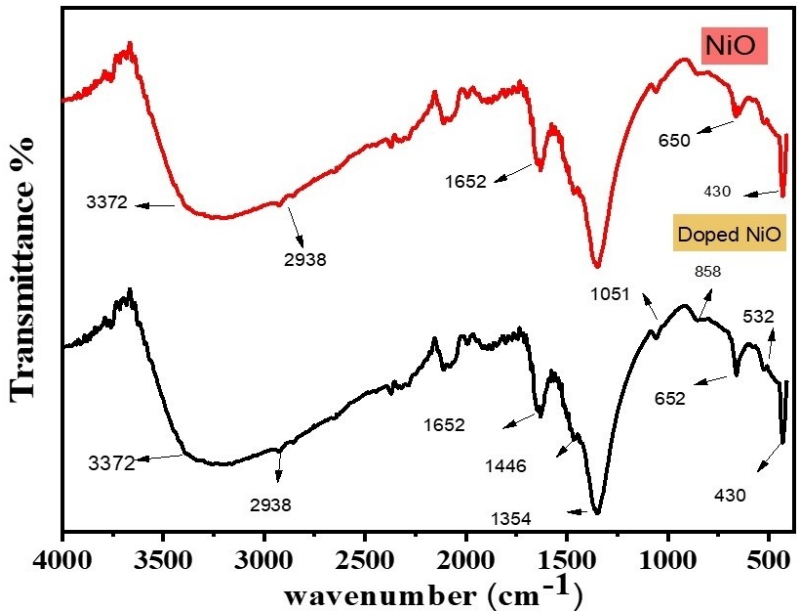

Figure 4. FTIR spectrum of NiO and co-doped (Mn, Zn) NPs illustrating the presence of different functional groups.

Table 1. Data showing the peaks of functional groups in pure and doped materials.		
Functional groups	Pure NiO NPs	Zn, Mn doped NPs
O–H, H–O-H bending vibrations	3372, 1652 cm ^{1}	3372, 1652 cm ^{1}
Hydroxyl ions	2938 cm ^{1}	2938 cm ^{1}
Oxides group	1446, 1051 cm ^{1}	1446, 1051 cm ^{1}
Lattice defects and enlargement	–	530–860 cm ^{1}
NiO vibrating mode	430 cm ^{1}	430 cm ^{1}

due to the presence of Zn and Mn metal ions in the lattice. Peak at 430 cm^{-1} corresponds to the Ni–O stretching vibration.[26,31–33]

X-ray diffraction (XRD) analysis

The crystal structure determination of NiO NPs and Zn/Mn co-doped NiO NPs was supported by XRD analysis. The XRD patterns of the nanomaterials showed the diffraction peaks at 37.1°, 43.2° and 62.5° corresponding to the (111), (200) and (220) crystalline planes. These peaks are well matched with JCPDS Card No. 04-0835 of NiO having the face centered cubic crystalline structures for both pure and doped particles (Figure 5). There were no extra phases inside the lattice even after the doping of metals.[34] However, the slight shift of peak at 43.2° for Zn/Mn co doped NiO was due to the large ionic size of the Zn^{2+} (0.74 Å) and Mn^{2+} (0.84 Å) as compared with the Ni^{2+} (0.6 Å) that expanded the unit cell. The broad peaks in the spectra with decreased intensity correspond to the decline in the crystallinity. No other metals peaks were detected, ensuring single phase NiO NPs without any impurity. The crystal size of the fabricated materials was estimated by Debye Scherer formula (Eq. 2).

$$D = \frac{k\lambda}{\beta \cos\theta} \tag{2}$$

Where, D denotes size of the crystal, λ is the wavelength of the X-ray light radiation, θ represented angle of diffraction and β is (FWHM) in radians. Size of the crystals was found to be 24 and 20 nm for pure NiO and Zn/Mn co-doped nanoparticles, respectively. A decrease in the crystalline size depicted the increase of the active sites, more energy levels with increased availability of electrons and holes playing their role in the photo-degradation reactions. Different parameters of pure and doped materials was illustrated by Table 2.

The W–H plots were used to evaluate the strain formed in pure and co doped particles (Figure 6 a, b). According to the W–H analysis, peak broadening is the sum of crystal size and lattice strain as shown in Eqs. 3 and 4.

$$\beta_{hkl=}\beta s + \beta_{d} \tag{3}$$

$$\beta_{hkl=}(k\lambda/D\cos\theta) + (4\varepsilon\sin\theta) \tag{4}$$

Where, k is a constant k = 0.94, λ = 1.5406 Å is the wavelength of X-rays, D is the crystal size, θ as the Bragg's angle, β_{hkl}

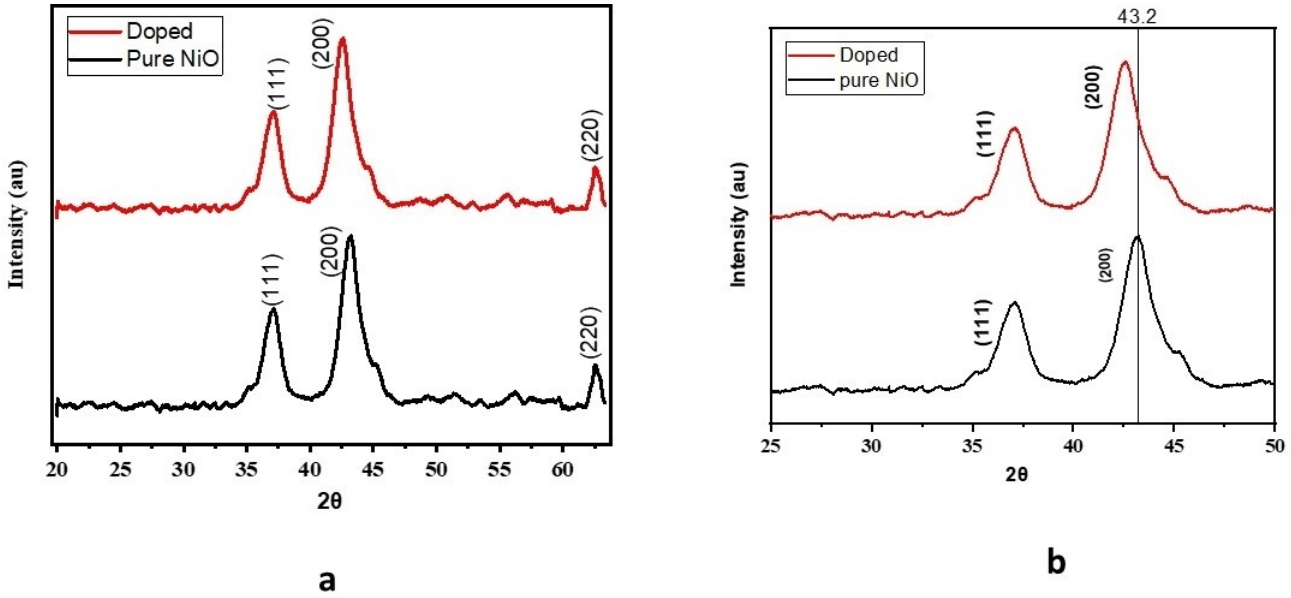

Figure 5. XRD pattern of (a) pure and co-doped material (b) zoomed XRD pattern illustrating the shifting of peak in doped and pure material.

Table 2. Different parameters of pure and doped material calculated from XRD analysis.		
	Pure NiO	Doped NiO
Lattice Constant (a)	3.499 nm	3.489 nm
X-Ray Density	2.32×10^{23} g/cm^3	2.32×10 g/cm^3
Strain	0.2400	0.2800
Dislocation density	0.10 g/cm^3	0.10 g/cm^3
Particle Size	24 nm	20 nm

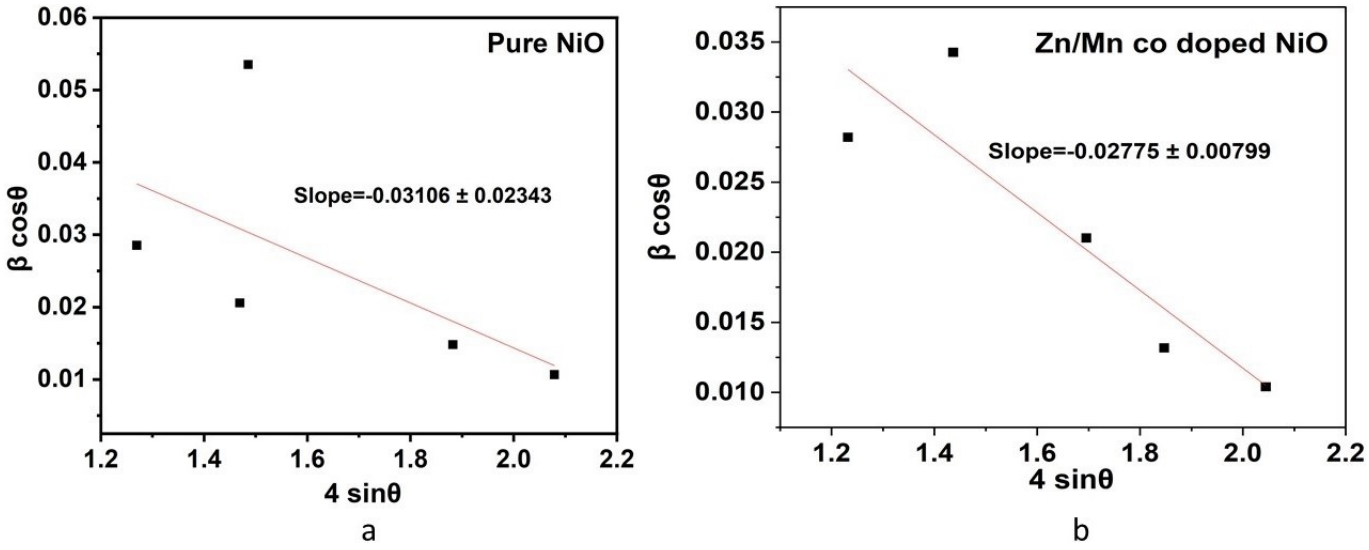

Figure 6. W–H plot of (a) pure NiO and (b) and doped NiO particles with their strain.

was the (FWHM) corresponding to Bragg's peak and ε = lattice strain. By rearranging, the equation 5 is obtained.

$$\beta_{hkl}\cos\theta = (k\lambda/D) + (4\varepsilon\sin\theta) \quad (5)$$

The graph was plotted between βcosθ and 4sinθ and strain was calculated. The negative values of the micro strain correspond to the smaller size of the crystals.[35] The W–H plot for pure NiO showed greater strain that was increased with the co doping of the NiO nanoparticles due to the lattice shrinkage.[36]

Dielectric studies

Dielectric constant

The dielectric properties of the pure NiO and Zn/Mn co-doped NiO NPs were studied by utilizing Impedance analyzer 6500 at standard conditions. The dielectric constant was calculated by Eq. 6.

$$\varepsilon' = Cd/A\varepsilon_o \quad (6)$$

Where, C represented the capacitance, d and A was the width and area of pallets, respectively. The ε_o denoted the vacuum permittivity having constant value of 8.85×10^{-2} F cm^{-1}. The dielectric constant measurements were evaluated by varying frequency values. From figure 7a, it can be inferred that Zn/Mn doped NiO NPs showed greater dielectric constant values in comparison to pure NiO NPs. As mentioned in literature, at low frequency region a dielectric material faced dipolar, interfacial electronic and atomic polarization effects. These polarizations lead to the escalating dielectric constant. However, at higher frequency region, only electronic and atomic polarizations exist and inhibits dielectric constant values. These results are very close to the already described literature.[37]

Dielectric loss constant

The imaginary dielectric constant of pure NiO and Zn/Mn co doped nanoparticles was exhibited in the (Figure 7b). The imaginary part (dielectric loss) actually showed the amount of energy dissipated. The dielectric loss was measured using Eq. 7:

$$\varepsilon'' = \varepsilon' \times \tan\delta \quad (7)$$

Where, ε′′ indicated the imaginary part of the dielectric constant which is inversely proportional to frequency and decreased in the value with the increase in the frequency. The

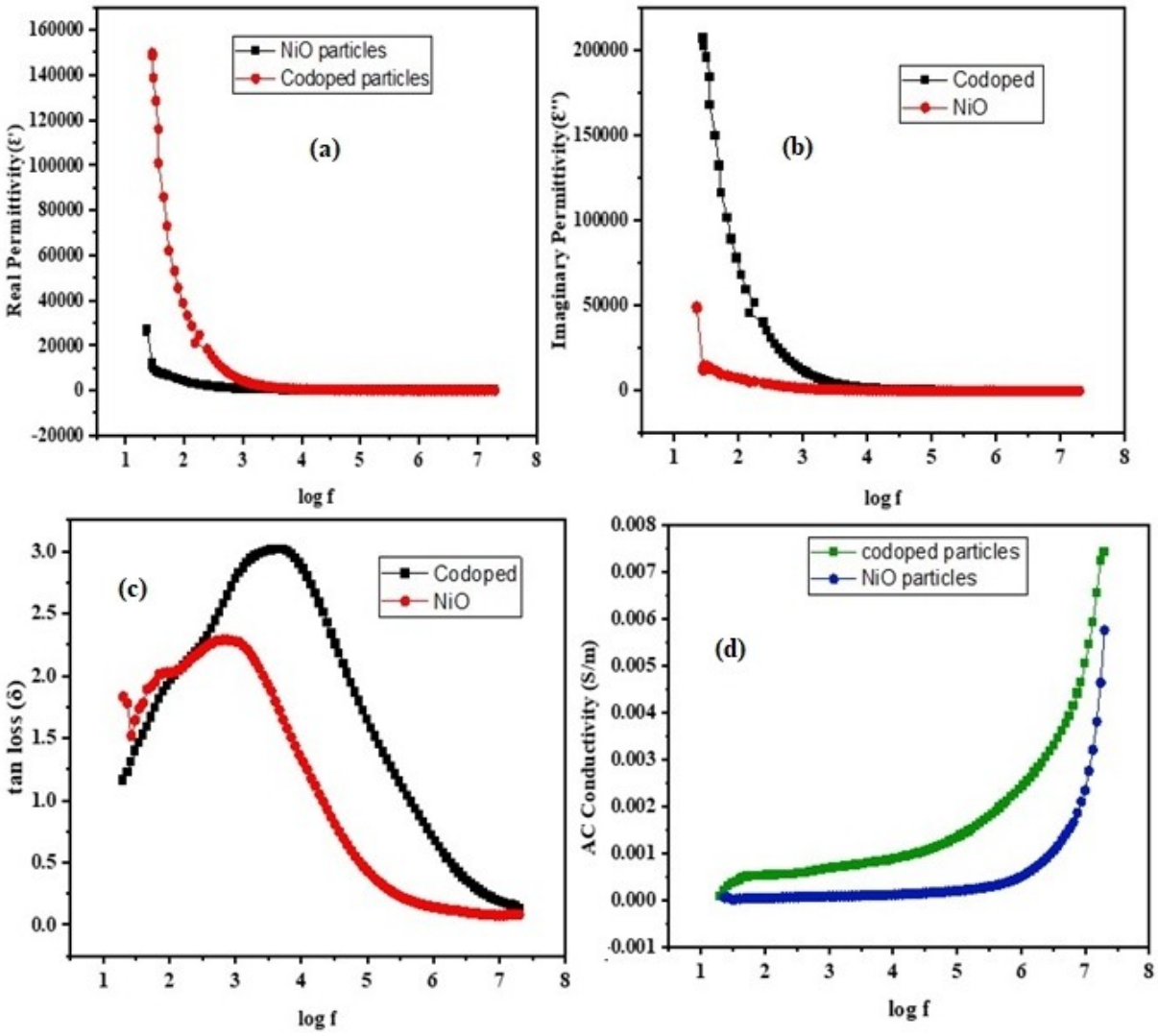

Figure 7. Plots of (a) real permittivity (b) imaginary permittivity (c) tangent loss (d) Effect of frequency on the AC conductivity of pure and co-doped NiO nanoparticles.

dielectric loss is found to be proportional to the energy dissipation. Hence, by doping of Zn and Mn, the increase in dielectric properties was observed which is attributed to the decline in the losses at the high frequency region.

Tangent loss

The energy dissipation and current out flow of the prepared materials were also described on the basis of tangent loss as shown in Eq. 8.

$$\tan\delta = 1/2\pi fRC \quad (8)$$

Where, f, C, and R depicted applied frequency, capacitance and resistance, respectively and π is a constant. The value of loss tan is higher at lowest frequency and low at high frequency and then, become constant. According to Koop's theory, tangent loss is an indication of potential required to transfer the electrical energy into thermal mode and doping of foreign material also induced defects in the structure, as it can be observed in figure 7c that the value of tangent loss is high at low frequency, which decreased by increasing the frequency. The decrease in tangent loss correlated to Maxwell-Wagner polarization along with conduction medium. After this, the tangent loss becomes constant because of domain wall motion inhibition. For a material to show efficient dielectric properties, it must have low energy loss (tangent loss) with high dielectric constant. The results of the present study well matched with this behavior, which reveals good dielectric properties.[38–40]

AC conductivity

The AC conductivity mainly relied on the movement of charge particles and was calculated by employing the following Eq. 9.

$$\rho_{ac} = 1/2\pi f \in '' \varepsilon_o \quad (9)$$

Where, f is the applied frequency, ε_o is the permittivity of vacuum and 'ε'' is the imaginary part of the permittivity (dielectric constant). Figure 7d clearly demonstrated constant conductivity value in the lower frequency range, which was gradually increased when moving to higher frequency region. An increase in frequency assigned to the enhanced movement of charges and ultimately, leads to high conductivity. These results are also in accordance to the reported studies.[15,41] According to the results Zn/Mn co doped NiO nanoparticles showed greater conductivity in comparison with pure NiO nanoparticles. Due to the introduction of Zn and Mn ions inside the lattice of host crystal, its dielectric property, charge storage capacity and conductivity has been increased.[42]

Photocatalytic activity

Effect of dye initial concentration

The experiment was carried out at neutral pH using MB dye concentration varying from 5 ppm to 20 ppm to check the impact of dye concentration on the PCA of the NiO NPs and Zn/Mn co-doped NiO NPs. The UV-visible spectra of dye before and after irradiation are shown in figure 8 and percentage dye degradation in figure 9a. For concentration of 5 ppm, the pure NiO degraded 70 % of dye in 60 min, while for Zn/Mn co doped NiO NPs, it was 90 % at irradiation time of 30 min. The dye degradation was 35 % and 20 % for the doped and pure sample as the amount of dye increased from 10 to 15 ppm, respectively. As the concentration of dye increased, the production of hydroxyl radicals (°OH) and UV light reaching the catalyst surface decreased leading to less photocatalytic activity. These factors contributed to the low efficiency of catalyst at high concentration of dye.[43]

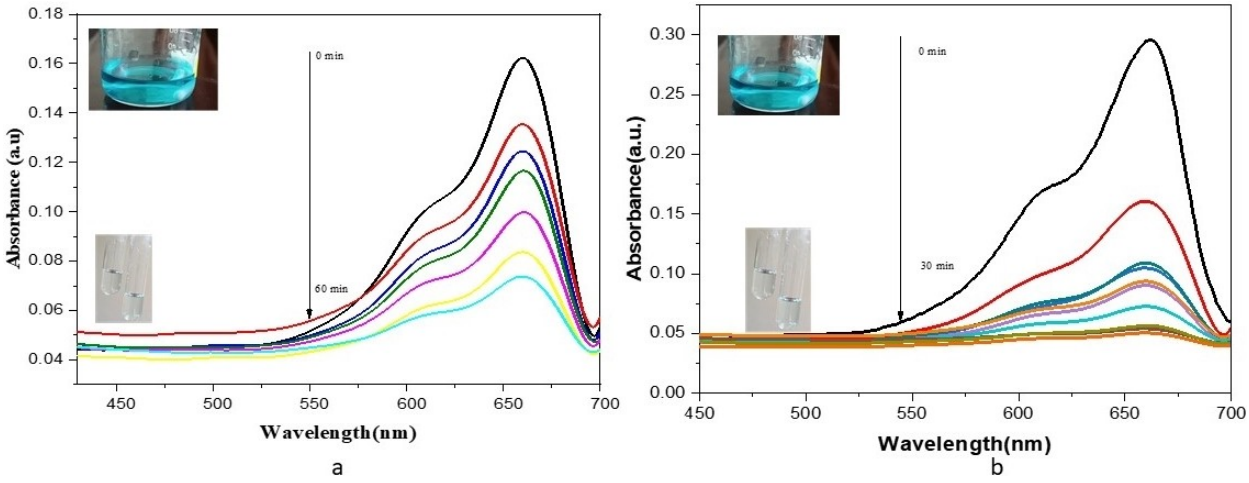

Figure 8. The UV-Visible spectra of dye before and after irradiation, (a) pure NiO NPs (b) co-doped NiO NPs.

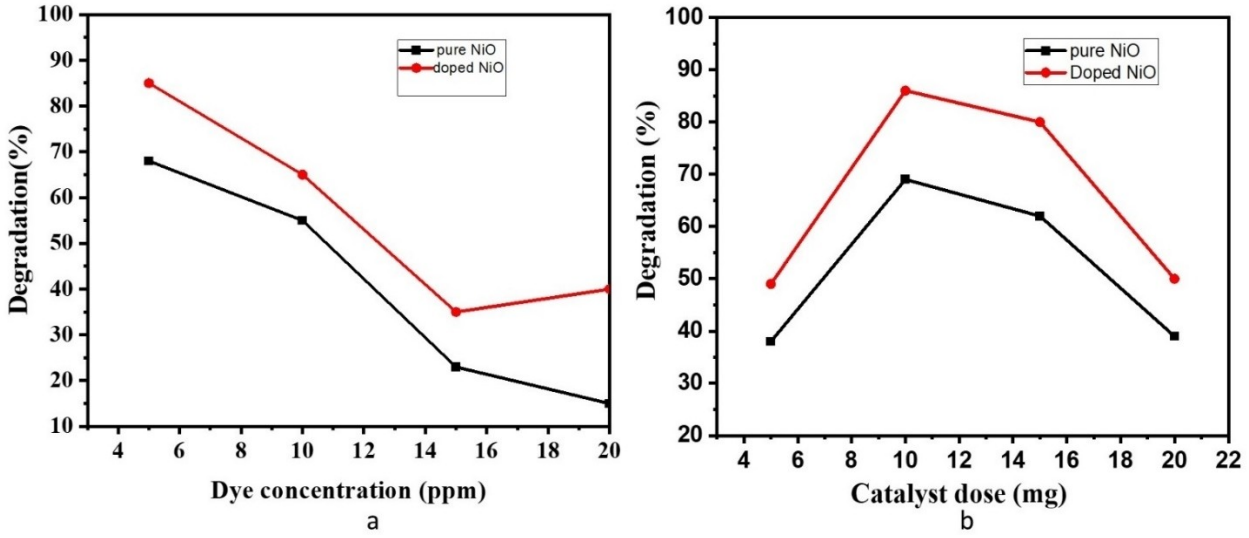

Figure 9. MB dye degradation as a function of (a) initial concentrations of dye (b) catalyst dose for pure NiO NPs and co-doped NiO NPs.

Catalyst dose

The effect of catalyst dosage was studied in 5–20 mg range for MB dye degradation by keeping all other conditions constant. From figure 9b, it was detected that the rate of degrading increased with the catalyst dose. As the availability of active sites enhanced the absorption of light and hence, higher the elimination of dye due to generation of higher hydroxyl radicals. As the amount of the catalyst increased up to 15 mg, the elimination of dye decreased because of the active sites being blocked due aggregates formation of the catalyst and reduction in the generation of hydroxyl radicals on the catalyst surface.[43,44]

Effect of pH

Medium pH performs a significant role in determining proficiency of the catalysts for the removal of dyes from water. Actually, the nature of dye and catalyst absorption capacity varied at different pH values of the medium. Thus, pH ranging from 3 to 12 was examined for the PCA of MB dye (Figure 10). In order to sustain the pH of the reaction medium, 0.1 M solution of NaOH and H_2SO_4 were used. The reaction was carried out with 5 ppm MB dye solution carrying 10 mg amount of the catalyst. The outcomes displayed the degradation efficiency increased with the increase in pH. At pH 12, the surface of the catalysts has large number of hydroxyl ions and MB being a cationic dye is being attracted more and destructed by the hydroxyl radicals. Percent removal of dye at this pH was found to 92% (30 min) and 70% (60 min) for Zn/Mn co doped NiO and pure NiO, respectively. Nevertheless, the less efficiency of the nanomaterials at low pH was due to the positive catalyst surface that declined the MB degradation owing to repulsion.[45]

Photocatalytic degradation mechanism

The photocatalytic degradation mechanism of MB dye one NiO photocatalyst is depicted in Figure 11. The Zn/Mn co doped NiO because of their low bandgap energy manifested better photodegradation reaction in comparison to pure NiO. Table 3 illustrated the comparison between the NiO based pure and doped materials with different metals for their photocatalytic activities. The chemical reaction involved in the dye degradation are explained in Eqs. 10–13. Accordingly, the holes are created due to excitation of electrons in response of incident light on the surface of the NiO semiconductor. The water molecules react with the holes on the catalyst surface that produce the of hydroxyl radicals ($^{\bullet}OH$). Furthermore, $O_2^{\bullet-}$ radicals are formed due to presence of electrons in the conduction band that reacts with O_2. These highly oxidized species, oxidize the MB dye molecules into H_2O, CO_2 and inorganic ions. These findings revealed that the prepared photocatalysts are highly active to degrade the dyes, which can be employed for the treatment of wastewater,[46] which is one of major issue due to anthropogenic activities.

Moreover, a scavenging experiment was conducted to gain insights into the photodegradation process of a dye and identify the most efficient species responsible for its removal. In

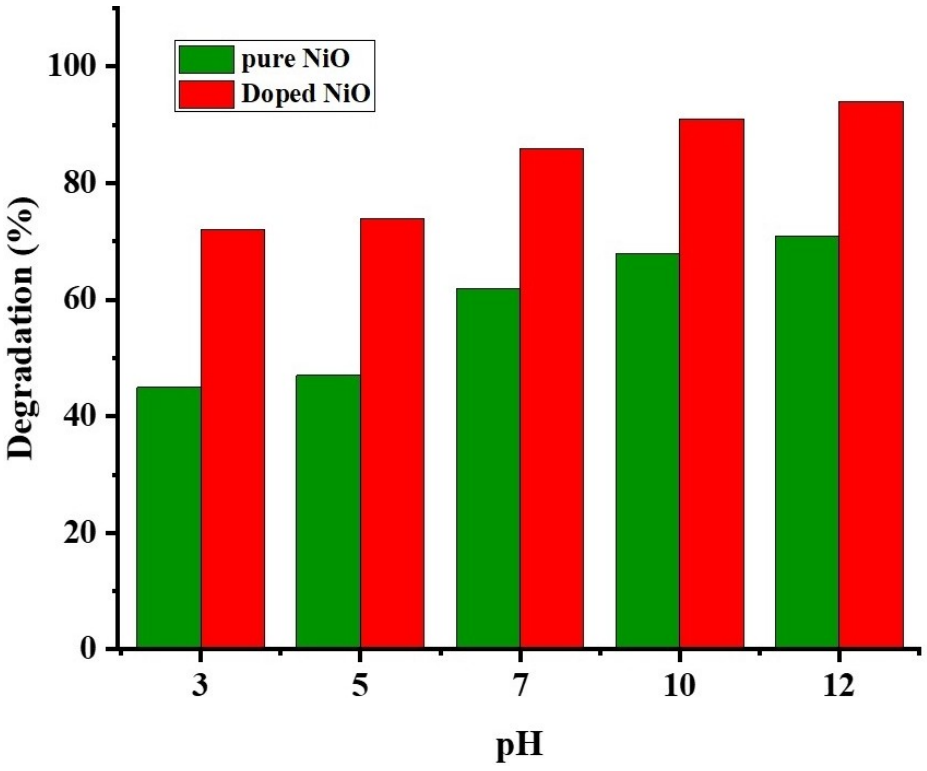

Figure 10. Plot showing the degradation of the dye at different pH.

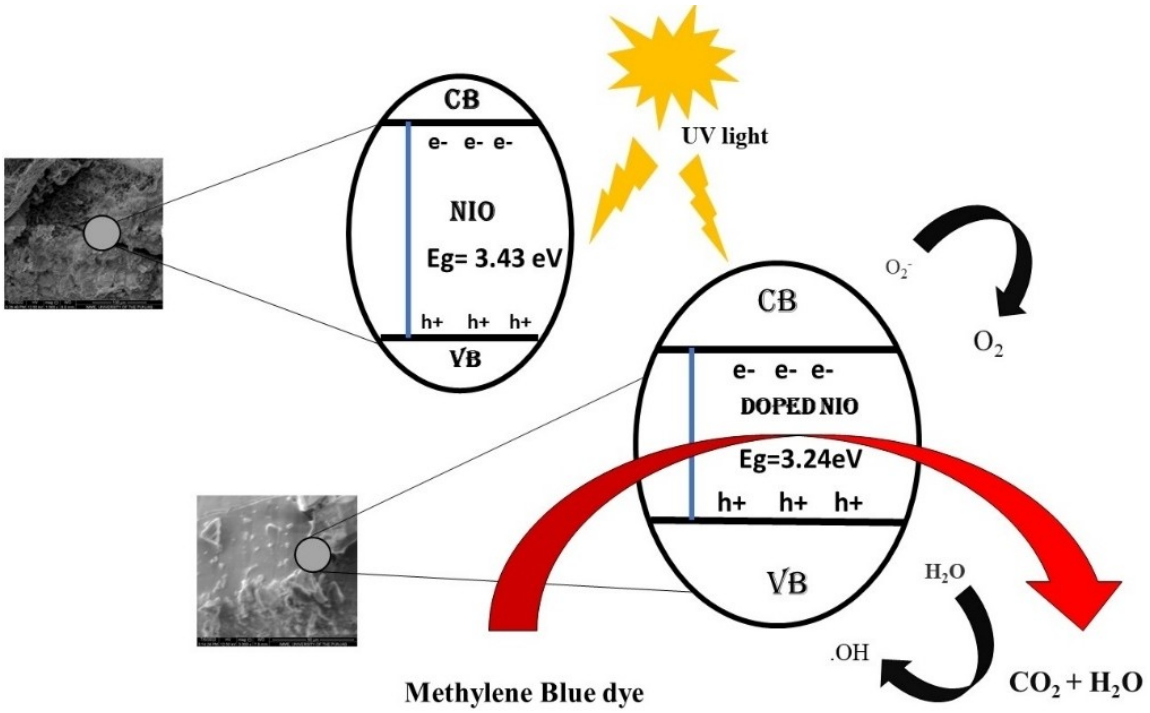

Figure 11. Mechanism of photocatalytic dye degradation.

Table 3. Comparative studies showing the photocatalytic degradation of dyes using NiO based catalysts.

Catalysts	Dye	Degradation (%)	Reference
Cu doped NiO NPs	MB	78	
Ag doped NiO NPs	RhB	75	
NiO NPs	MB	65.5	
RGO/NiO NC	MB	93/65	
Mn, Zn doped NiO	MB	94	Present work
NiO NPs	**MB**	**70**	**Present work**

the quest to understand the degradation mechanism, the formation of active species, namely hydroxyl radicals, holes, and electrons, was found to play a vital role in the breakdown of dyes. To delve deeper into the roles of these active species, a scavenging experiment was devised with the utilization of different trapping agents: 2-propanol for hydroxyl radicals, EDTA for holes, and $AgNO_3$ for electrons. The experiment's outcomes, depicted in figure 12, showing dye degradation percentages of 21%, 42%, 58%, and 94% in the presence of 2-propanol, EDTA, $AgNO_3$, and no scavenger, respectively. Upon careful analysis of the scavenging studies, a compelling pattern emerged. It became evident that the degradation rate was notably lower when hydroxyl radicals were effectively trapped, followed by the trapping of holes and electrons. This observation led to the establishment of an order of effectiveness for the different active species in the dye degradation process: hydroxyl radicals $>$ holes $>$ electrons. The significance of hydroxyl radicals in the degradation of the dye became prominently clear, highlighting their major role in driving the photodegradation process. These findings shed light on the intricate interplay of active species during dye degradation and underscore the importance of hydroxyl radicals as the primary contributors to the breakdown of the dye molecules. Understanding the roles and relative significance of these active species is of utmost importance in devising efficient and sustainable dye degradation strategies. This knowledge can be leveraged to optimize photocatalytic processes, ultimately leading to enhanced environmental remediation and wastewater treatment applications.

$$\text{Photocatalyst} + hv \rightarrow h_{VB}^{+} + e_{CB} \quad (10)$$

$$H2O + hVB+ \rightarrow {}^{\bullet}OH\ (\text{hydroxyl radical}) + H+ \quad (11)$$

$$O_2 + e_{CB} \rightarrow O_2^{\bullet}\ \ (\text{Super oxide radical}) \quad (12)$$

$$^{\bullet}OH + \text{dye} \rightarrow \text{Intermediates} \rightarrow {}^{\bullet}H2O + CO2 + \text{other mineralized products} \quad (13)$$

Recycling studies of pure and co-doped NiO NPs

In order to explore the recyclability of the prepared catalysts, the recycling studies were conducted (Figure 13). The catalyst was collected from the first cycle, separated, dried and reused for the next cycle, which was repeated up to four cycles. For pure NiO nanoparticles, a 71% degradation for initial run was observed, which was dropped to 46%. The co-doped NiO NPs initially degraded 94% of dye, which decreased to 62% after four consecutive cycles. The decrease in the activity was due to

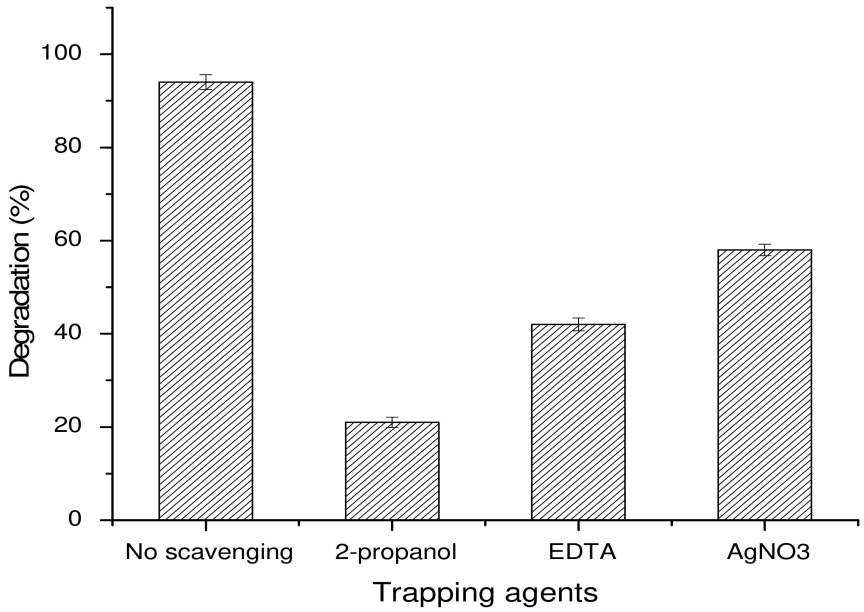

Figure 12. Scavenging studies in the presence of different agents.

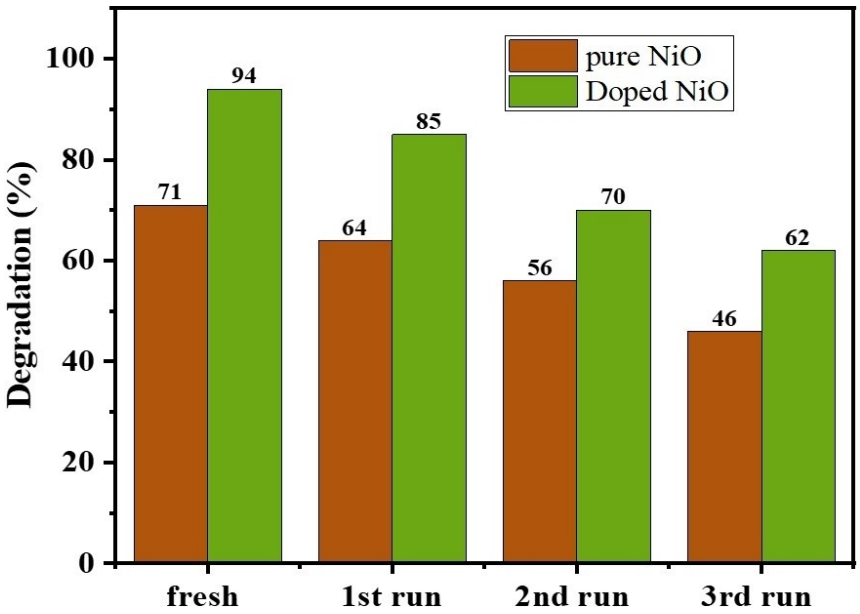

Figure 13. Recycling performance of pure NiO NPs and co-doped NiO NPs.

loss in active sites.[47–49] Recycling research on photocatalysts has several benefits and is essential for developing photocatalytic technology and environmental sustainability. The preservation of resources, cost effectiveness, diminished environmental impact, and waste reduction are a few of the major advantages. We can increase photocatalysts' durability and efficacy across several cycles by recycling them. Additionally, research on recycling fosters technological innovation, which results in the creation of new materials and methods for photocatalytic processes that are both more efficient and sustainable. This adds to the idea of a circular economy, which eliminates the need for linear production and waste creation by continuously reusing materials. Overall, research on recycling photocatalysts has the potential to completely transform the field of photocatalysis, making it a more sustainable and environmentally friendly method of addressing numerous environmental issues and fostering a more sustainable future.

Conclusions

A sol- gel method was successfully employed for the preparation of pure NiO and Zn/Mn co-doped NiO NPs. The synthesized materials were characterized using UV-Vis., FTIR, SEM, EDX and

XRD. The dielectric properties were improved of NiO due to Zn and Mn doping along with optical properties. These photocatalytic removal of MB dye was studied as a function of dye concentration, pH of the solution, contact time and effect of the catalyst dose. The best removal percentage (94%) was obtained for Zn/Mn co doped NiO NPs at pH 12 under UV irradiation in only 30 min of irradiation, which was significantly higher than the pure NiO NPs. These results clearly demonstrated that Zn/Mn co-doped NiO NPs is efficient photocatalyst for the removal of dye versus pure NiO NPs, which could be employed for the remediation of dyes in effluents. Future studies can be focused on the photocatalytic activity under solar light irradiation, which will more economical versus UV light based photocatalytic process.

Experimental Section

All the chemicals and reagents used in this study were of analytical grade and were purchased from Sigma Aldrich. Nickel chloride ($NiCl_2 \cdot 6H_2O$), citric acid ($C_6\ H_8\ O_7$), sodium hydroxide (NaOH), zinc nitrate ($Zn\ (NO_3)_2 \cdot 6H_2O$) and manganese chloride ($MnCl_2.\ 4H_2O$) obtained from Sigma Aldrich and methylene blue dye was purchased from Merck.

Synthesis of Zn/Mn co doped NiO

Zn/Mn co-doped NiO NPs was synthesized sol gel method and a overall, presentation is depicted in Figure 14. A 0.2 M of nickel chloride hexahydrate and 0.02 M of citric acid was added in 50 mL of distilled water and the mixture was stirred for 30 min vigorously. Then, 0.02 M of zinc nitrate and 0.02 M of manganese chloride was also dissolved. Later, 2 M NaOH was added dropwise to achieve the basic pH (>11). The green solution obtained was heated at 80 °C until it was converted into a gel. Water, ethanol and acetone were then used to wash the gel by centrifugation at 3000 rpm for 20 min to attain neutral pH. The sample placed in oven for drying for 3 h at 100 °C and then calcination was carried out at 350 °C for 2 h in a muffle furnace. For the synthesis of pure NiO nanoparticles the same procedure was repeated except the addition of Mn an Zn.[50]

Characterization

X-ray diffraction analysis was done using X-ray diffractometer (Rigaku D/ Max 2500 VBZ + PC) at 298 K over the 2θ ranges from 20° to 65° using Cu Kα Radiation source. FTIR spectroscopic analysis was done by Cary 630 FTIR Spectrometer in the range of 400–4000 cm^{-1}. Ultraviolet-visible (UV-Vis) analysis of the nanoparticles was carried out on a UV-Vis spectrophotometer (T 90 + spectrophotometer). The SEM and EDX was done at MIRA3 TESCAN operated at the voltage of 10 KV.

Photocatalytic activity (PCA)

To check the PCA of the prepared samples was studied for MB dye under UV light irradiation. Ultraviolet radiation is provided by 70 W mercury lamp. A 50 mL of 5 ppm dye solution was taken and 10 mg of sample (nanoparticles) was added in it. The sample was stirred in dark for 15 minutes and then, subjected to UV light. After the certain time, sample was withdrawn and centrifuged. The particles of catalyst were settled down, the supernatant solution was taken out and absorbance was measured at 664 nm (CE Celil UK) and dye degradation percentage was measured using Eq. 14.

$$\text{Degradation } (\%) = \frac{A_0 - A_t}{A_0} \times 100 \tag{14}$$

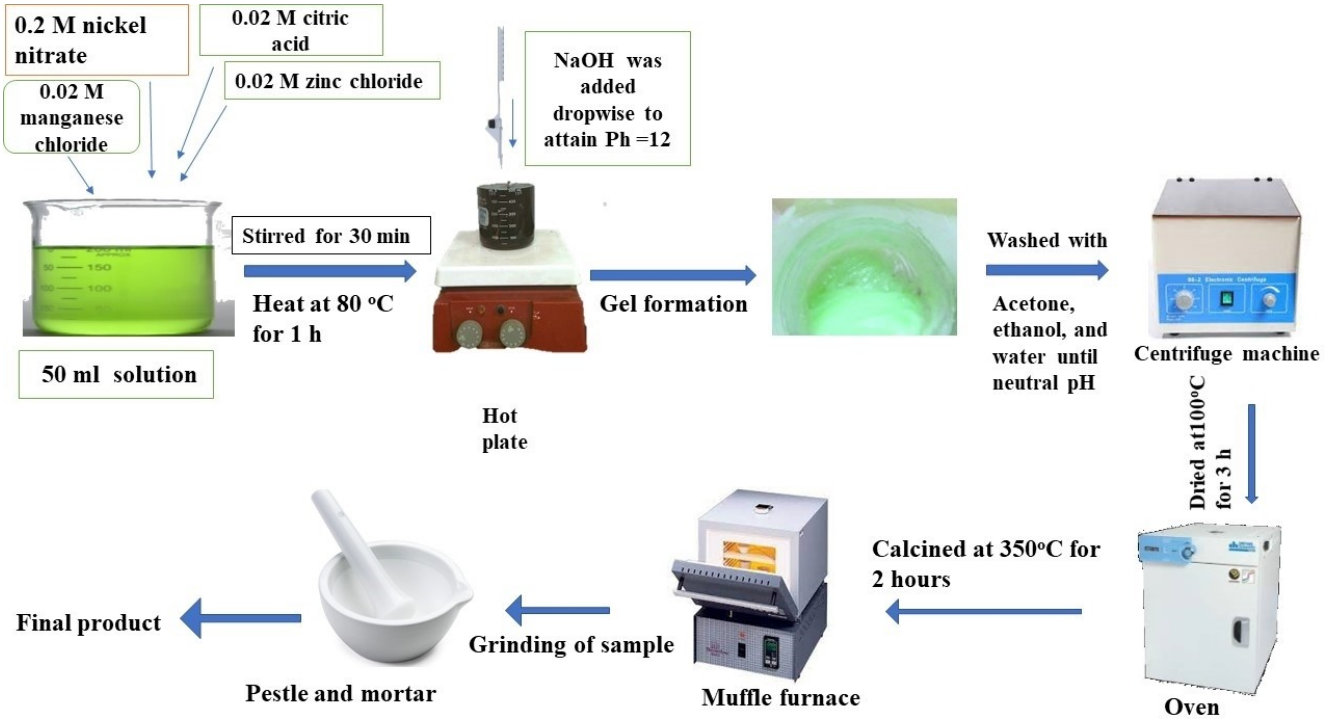

Figure 14. Schematic diagram for the synthesis of (Mn, Zn) co-doped NiO nanoparticles.

where, A_0 and A_t were the initial and the final absorbance respectively taken after a degradation at that particular time.

Funding statement

This research was funded by Princess Nourah bint Abdulrahman University Researchers Supporting Project number (PNURSP2023R11), Princess Nourah bint Abdulrahman University, Riyadh, Saudi Arabia.

Acknowledgements

The authors express their gratitude to Princess Nourah bint Abdulrahman University Researchers Supporting Project number (PNURSP2023R11), Princess Nourah bint Abdulrahman University, Riyadh, Saudi Arabia.

Conflict of Interests

The authors declare that they have no known competing financial interests or personal relationships that could have appeared to influence the work reported in this paper.

Data Availability Statement

Data will be made available upon request.

Keywords: Nickel oxide · Zn–Mn doping · Dielectric properties · Photocatalytic activity · Dye degradation

[1] R. Mehrkhah, K. Goharshadi, E. K. Goharshadi, H. S. Sajjadizadeh, *ChemistrySelect* **2023**, *8*, e202204386.
[2] H. Wan, Q. Huang, R. Mia, X. Tao, S. Mahmud, H. Liu, *ChemistrySelect* **2022**, *7*, e202200649.
[3] M. Usman, M. Adnan, S. Ali, S. Javed, M. A. Akram, *ChemistrySelect* **2020**, *5*, 12618–12623.
[4] N. Abbas, N. Hussain, U. F. Gohar, F. Zaheer, M. Hamza, M. Yasir, A. Abbas, *Chem. Int.* **2022**, *8*, 114–129.
[5] M. Iqbal, M. Abbas, J. Nisar, A. Nazir, A. Qamar, *Chem. Int.* **2019**, *5*, 1–80.
[6] D. Idika, N. Ndukwe, C. Ogukwe, *Chem. Int.* **2022**, *8*, 42–46.
[7] G. Jalal, N. Abbas, F. Deeba, T. Butt, S. Jilal, S. Sarfraz, G. Jalal, N. Abbas, F. Deeba, T. Butt, S. Jilal, S. Sarfraz, *Chem. Int.* **2021**, *7*, 197–207.
[8] K. Elsherif, A. El-Dali, A. Alkarewi, A. Ewlad-Ahmed, A. Treban, *Chem. Int.* **2021**, *7*, 79–89.
[9] S. Landi Jr., J. Carneiro, S. Ferdov, A. M. Fonseca, I. C. Neves, M. Ferreira, P. Parpot, O. S. G. P. Soares, M. F. R. Pereira, *J. Photochem. Photobiol. A* **2017**, *346*, 60–69.
[10] M. Laissaoui, Y. Elbatal, I. Vioque, G. Manjon, *Chem. Int.* **2017**, *3*, 343–352.
[11] A. Kausar, S. T. Zohra, S. Ijaz, M. Iqbal, J. Iqbal, I. Bibi, S. Nouren, N. El Messaoudi, A. Nazir, *Int. J. Biol. Macromol.* **2023**, *224*, 1337–1355.
[12] U. H. Siddiqua, S. Ali, M. Iqbal, T. Hussain, *J. Mol. Liq.* **2017**, *241*, 839–844.
[13] F. Minas, B. S. Chandravanshi, S. Leta, *Chem. Int.* **2017**, *3*, 291–305.
[14] Z. Nazeer, I. Bibi, F. Majid, S. Kamal, S. M. Ibrahim, M. Iqbal, *Opt. Mater.* **2022**, *125*, 112090.
[15] S. Iqbal, I. Bibi, F. Majid, S. Kamal, N. Alwadai, M. Iqbal, *Opt. Mater.* **2022**, *124*, 111962.
[16] B. Ahmad, M. I. Khan, M. A. Naeem, A. Alhodaib, M. Fatima, M. Amami, E. A. Al-Abbad, A. Kausar, N. Alwadai, A. Nazir, M. Iqbal, *Mater. Chem. Phys.* **2022**, *288*, 126363.
[17] S. M. Aydoghmish, S. A. Hassanzadeh-Tabrizi, A. Saffar-Teluri, *Ceram. Int.* **2019**, *45*, 14934–14942.
[18] A. Miri, F. Mahabbati, A. Najafidoust, M. J. Miri, M. Sarani, *Inorg. Nano-Met. Chem.* **2022**, *52*, 122–131.
[19] A. Khatri, P. S. Rana, *Phys. B: Cond. Matt.* **2020**, *579*, 411905.
[20] M. A. Rahman, R. Radhakrishnan, R. Gopalakrishnan, *J. Alloy. Comp.* **2018**, *742*, 421–429.
[21] M. I. Din, R. Khalid, Z. Hussain, *Anal. Lett.* **2018**, *51*, 892–907.
[22] J. Al Boukhari, L. Zeidan, A. Khalaf, R. Awad, *Chem. Phys.* **2019**, *516*, 116–124.
[23] Y.-C. Chen, K.-i. Katsumata, Y.-H. Chiu, K. Okada, N. Matsushita, Y.-J. Hsu, *Appl. Catal. A* **2015**, *490*, 1–9.
[24] M. Barman, S. Paul, A. Sarkar, *American Institute of Physics*, p. 427–428.
[25] S. Dewan, M. Tomar, R. P. Tandon, V. Gupta, *J. Appl. Phys.* **2017**, *121*, 215307.
[26] Z. Nazeer, I. Bibi, F. Majid, S. Kamal, M. I. Arshad, A. Ghafoor, N. Alwadai, A. Ali, A. Nazir, M. Iqbal, *ACS Omega* **2023**, *8*, 24980.
[27] N. Khaliq, I. Bibi, F. Majid, M. Sultan, M. Amami, M. Iqbal, *Mater. Sci. Semicond. Process.* **2022**, *139*, 106324.
[28] B. A. Josephine, A. Manikandan, V. M. Teresita, S. A. Antony, *Korean J. Chem. Eng.* **2016**, *33*, 1590–1598.
[29] X. Wan, M. Yuan, S.-l. Tie, S. Lan, *Appl. Surf. Sci.* **2013**, *277*, 40–46.
[30] H. T. Rahal, R. Awad, A. M. Abdel-Gaber, D. Bakeer, *J. Nanomater.* **2017**, *2017*, 7460323.
[31] S. Sankar, S. K. Sharma, N. An, H. Lee, D. Y. Kim, Y. B. Im, Y. D. Cho, R. S. Ganesh, S. Ponnusamy, P. Raji, *Optik* **2016**, *127*, 10727.
[32] Q. Raza, I. Bibi, F. Majid, S. Kamal, S. Ata, A. Ghafoor, M. I. Arshad, S. H. Al-Mijalli, A. Nazir, M. Iqbal, *J. Ind. Eng. Chem.* **2023**, *118*, 469–482.
[33] S. Muqaddas, H. Aslam, S. Ul Hassan, A. Raza Ashraf, M. Adeel Asghar, M. Ahmad, A. Nazir, R. Shoukat, M. Kaleli, S. Mostafa Ibrahim, S. Kyürekli, A. Haider, A. Ali, *Mater. Sci. Eng. B.* **2023**, *293*, 116446.
[34] Z. Bitar, S. Isber, S. Noureddine, D. E.-S. Bakeer, R. Awad, *J. Supercond. Novel Magn.* **2017**, *30*, 3603–3609.
[35] K. Maniammal, G. Madhu, V. Biju, *Phys. E: Low-dimen. Sys. Nanostr.* **2017**, *85*, 214–222.
[36] S. Jaidka, S. Khan, K. Singh, *Phys. B: Cond. Matt.* **2018**, *550*, 189–198.
[37] F. Majid, I. Wahid, S. Ata, I. Bibi, M. D. Ali, A. Malik, N. Alwadai, M. Iqbal, A. Nazir, *Mater. Chem. Phys.* **2021**, *264*, 124451.
[38] A. Ghafoor, I. Bibi, F. Majid, S. Kamal, K. Jilani, M. Sultan, N. Alwadai, A. Ali, A. Ali, A. Nazir, M. Iqbal, *Mater. Sci. Semicond. Process.* **2023**, *160*, 107408.
[39] A. Nazir, F. Khalid, S. u. Rehman, M. Sarwar, M. Iqbal, M. Yaseen, M. Iftikhar Khan, M. Abbas, *Z. Phys. Chem.* **2021**, *235*, 769–784.
[40] I. Bibi, H. Sabir, M. Farzana, K. Shagufta, A. Sadia, S. Misbah, D. Muhammad Imran, I. Munawar, A. Nazir, *Z. Phys. Chem.* **2019**, *233*, 1431–1445.
[41] S. K. Gore, S. S. Jadhav, U. B. Tumberphale, S. M. Shaikh, M. Naushad, R. S. Mane, *Solid State Sci.* **2017**, *74*, 88–94.
[42] Z. Anwar, M. A. Khan, I. Ali, M. Asghar, M. Sher, I. Shakir, M. Sarfraz, M. F. Warsi, *J. Ovonic Res.* **2014**, *10*, 265–273.
[43] I. Bibi, T. Naz, F. Majid, S. Kamal, S. Ata, M. M. Almoneef, S. Iqbal, M. Iqbal, *Int. J. Energy Res.* **2021**, *45*, 11193–11205.
[44] A. Ghafoor, I. Bibi, S. Ata, F. Majid, S. Kamal, M. Iqbal, S. Iqbal, S. Noureen, B. Basha, N. Alwadai, *J. Mol. Liq.* **2021**, *343*, 117581.
[45] S. Noreen, S. Ismail, S. M. Ibrahim, H. S. Kusuma, A. Nazir, M. Yaseen, M. I. Khan, M. Iqbal, *Z. Phys. Chem.* **2021**, *235*, 1055–1075.
[46] F. Deeduah, G. Iwuoha, D. F. Mene, G. N. Iwuoha, *Chem. Int.* **2021**, *7*, 217–223.
[47] S. Ghazal, A. Akbari, H. A. Hosseini, Z. Sabouri, F. Forouzanfar, M. Khatami, M. Darroudi, *Appl. Phys. A* **2020**, *126*, 1–8.
[48] Q. Kanwal, S. Shahid, A. Ahmad, A. Nazir, M. Yasir, A. Anwar, S. Z. Alshawwa, M. Iqbal, *Environ. Res.* **2023**, *233*, 116477.
[49] Z. Iqbal, M. Imran, S. Latif, A. Nazir, S. M. Ibrahim, I. Ahmad, M. Iqbal, S. Iqbal, *Z. Phys. Chem.* **2023**, *237*, 1139–1152.
[50] A. Chinnathambi, S. A. Alharbi, R. Lavarti, G. K. Jhanani, R. On-Uma, K. Jutamas, W. Anupong, *Environ. Res.* **2023**, *216*, 114574.